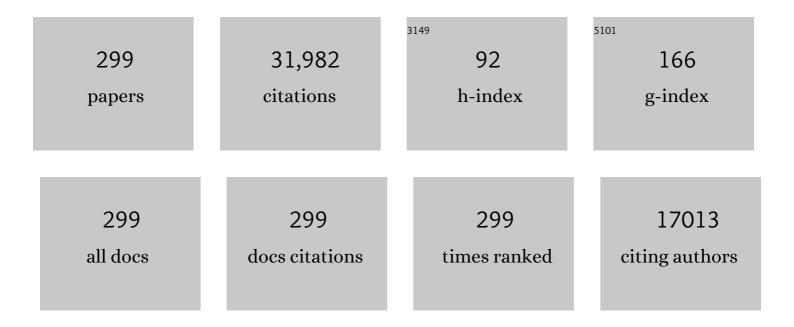
List of Publications by Year in descending order

Source: https://exaly.com/author-pdf/9356646/publications.pdf Version: 2024-02-01



ΥλΝΙΠΑΝ STIN

#	Article	IF	CITATIONS
1	Graphitic carbon nitride based nanocomposites: a review. Nanoscale, 2015, 7, 15-37.	2.8	1,440
2	In Situ Construction of g-C <sub>3</sub> N <sub>4</sub> /g-C <sub>3</sub> N <sub>4</sub> Metal-Free Heterojunction for Enhanced Visible-Light Photocatalysis. ACS Applied Materials & Interfaces, 2013, 5, 11392-11401.	4.0	1,102
3	Efficient synthesis of polymeric g-C3N4 layered materials as novel efficient visible light driven photocatalysts. Journal of Materials Chemistry, 2011, 21, 15171.	6.7	940
4	Bridging the g-C <sub>3</sub> N <sub>4</sub> Interlayers for Enhanced Photocatalysis. ACS Catalysis, 2016, 6, 2462-2472.	5.5	869
5	Anionic Group Self-Doping as a Promising Strategy: Band-Gap Engineering and Multi-Functional Applications of High-Performance CO <sub>3</sub> <sup>2–</sup> -Doped Bi <sub>2</sub> O <sub>2</sub> CO <sub>3</sub> . ACS Catalysis, 2015, 5, 4094-4103.	5.5	690
6	In situ assembly of BiOI@Bi 12 O 17 Cl 2 p - n junction: charge induced unique front-lateral surfaces coupling heterostructure with high exposure of BiOI {001} active facets for robust and nonselective photocatalysis. Applied Catalysis B: Environmental, 2016, 199, 75-86.	10.8	577
7	Threeâ€inâ€One Oxygen Vacancies: Whole Visibleâ€Spectrum Absorption, Efficient Charge Separation, and Surface Site Activation for Robust CO <sub>2</sub> Photoreduction. Angewandte Chemie - International Edition, 2019, 58, 3880-3884.	7.2	483
8	An Advanced Semimetal–Organic Bi Spheres– <i>g</i> -C <sub>3</sub> N <sub>4</sub> Nanohybrid with SPR-Enhanced Visible-Light Photocatalytic Performance for NO Purification. Environmental Science & Technology, 2015, 49, 12432-12440.	4.6	473
9	Noble Metal-Like Behavior of Plasmonic Bi Particles as a Cocatalyst Deposited on (BiO) <sub>2</sub> CO <sub>3</sub> Microspheres for Efficient Visible Light Photocatalysis. ACS Catalysis, 2014, 4, 4341-4350.	5.5	441
10	Immobilization of Polymeric g-C <sub>3</sub> N <sub>4</sub> on Structured Ceramic Foam for Efficient Visible Light Photocatalytic Air Purification with Real Indoor Illumination. Environmental Science & Technology, 2014, 48, 10345-10353.	4.6	436
11	Enhanced visible light photocatalytic activity and oxidation ability of porous graphene-like g-C3N4 nanosheets via thermal exfoliation. Applied Surface Science, 2015, 358, 393-403.	3.1	378
12	Enhancement of the Visible Light Photocatalytic Activity of C-Doped TiO <sub>2</sub> Nanomaterials Prepared by a Green Synthetic Approach. Journal of Physical Chemistry C, 2011, 115, 13285-13292.	1.5	365
13	Engineering the nanoarchitecture and texture of polymeric carbon nitride semiconductor for enhanced visible light photocatalytic activity. Journal of Colloid and Interface Science, 2013, 401, 70-79.	5.0	358
14	Bi <sub>2</sub> O <sub>2</sub> (OH)(NO <sub>3</sub> ) as a desirable [Bi <sub>2</sub> O <sub>2</sub> ] <sup>2+</sup> layered photocatalyst: strong intrinsic polarity, rational band structure and {001} active facets co-beneficial for robust photooxidation capability. Journal of Materials Chemistry A, 2015, 3, 24547-24556.	5.2	352
15	Room temperature synthesis and highly enhanced visible light photocatalytic activity of porous BiOI/BiOCI composites nanoplates microflowers. Journal of Hazardous Materials, 2012, 219-220, 26-34.	6.5	333
16	Water-assisted production of honeycomb-like g-C <sub>3</sub> N <sub>4</sub> with ultralong carrier lifetime and outstanding photocatalytic activity. Nanoscale, 2015, 7, 2471-2479.	2.8	328
17	Chlorine intercalation in graphitic carbon nitride for efficient photocatalysis. Applied Catalysis B: Environmental, 2017, 203, 465-474.	10.8	328
18	Template-free precursor-surface-etching route to porous, thin g-C <sub>3</sub> N <sub>4</sub> nanosheets for enhancing photocatalytic reduction and oxidation activity. Journal of Materials Chemistry A, 2017, 5, 17452-17463.	5.2	324

#	Article	IF	CITATIONS
19	In situ co-pyrolysis fabrication of CeO <sub>2</sub> /g-C <sub>3</sub> N <sub>4</sub> n–n type heterojunction for synchronously promoting photo-induced oxidation and reduction properties. Journal of Materials Chemistry A, 2015, 3, 17120-17129.	5.2	319
20	Hybridization of rutile TiO2 (rTiO2) with g-C3N4 quantum dots (CN QDs): An efficient visible-light-driven Z-scheme hybridized photocatalyst. Applied Catalysis B: Environmental, 2017, 202, 611-619.	10.8	296
21	Rational design on 3D hierarchical bismuth oxyiodides via in situ self-template phase transformation and phase-junction construction for optimizing photocatalysis against diverse contaminants. Applied Catalysis B: Environmental, 2017, 203, 879-888.	10.8	289
22	Rare-Earth Single-Atom La–N Charge-Transfer Bridge on Carbon Nitride for Highly Efficient and Selective Photocatalytic CO <sub>2</sub> Reduction. ACS Nano, 2020, 14, 15841-15852.	7.3	283
23	A semimetal bismuth element as a direct plasmonic photocatalyst. Chemical Communications, 2014, 50, 10386-10389.	2.2	282
24	Identification of Halogen-Associated Active Sites on Bismuth-Based Perovskite Quantum Dots for Efficient and Selective CO <sub>2</sub> -to-CO Photoreduction. ACS Nano, 2020, 14, 13103-13114.	7.3	282
25	Single-unit-cell layer established Bi2WO6 3D hierarchical architectures: Efficient adsorption, photocatalysis and dye-sensitized photoelectrochemical performance. Applied Catalysis B: Environmental, 2017, 219, 526-537.	10.8	264
26	Synthesis of Bi2WO6 with gradient oxygen vacancies for highly photocatalytic NO oxidation and mechanism study. Chemical Engineering Journal, 2019, 361, 129-138.	6.6	262
27	One-Step "Green―Synthetic Approach for Mesoporous C-Doped Titanium Dioxide with Efficient Visible Light Photocatalytic Activity. Journal of Physical Chemistry C, 2009, 113, 16717-16723.	1.5	260
28	Nitrogen defect structure and NO+ intermediate promoted photocatalytic NO removal on H2 treated g-C3N4. Chemical Engineering Journal, 2020, 379, 122282.	6.6	260
29	Facile transformation of low cost thiourea into nitrogen-rich graphitic carbon nitride nanocatalyst with high visible light photocatalytic performance. Catalysis Science and Technology, 2012, 2, 1332.	2.1	253
30	Identification of Active Hydrogen Species on Palladium Nanoparticles for an Enhanced Electrocatalytic Hydrodechlorination of 2,4-Dichlorophenol in Water. Environmental Science & Technology, 2017, 51, 7599-7605.	4.6	249
31	Characterization and photocatalytic activities of C, N and S co-doped TiO <sub>2</sub> with 1D nanostructure prepared by the nano-confinement effect. Nanotechnology, 2008, 19, 365607.	1.3	247
32	Visible-light-induced charge transfer pathway and photocatalysis mechanism on Bi semimetal@defective BiOBr hierarchical microspheres. Journal of Catalysis, 2018, 357, 41-50.	3.1	246
33	Highly enhanced visible light photocatalysis and in situ FT-IR studies on Bi metal@defective BiOCl hierarchical microspheres. Applied Catalysis B: Environmental, 2018, 225, 218-227.	10.8	238
34	Local spatial charge separation and proton activation induced by surface hydroxylation promoting photocatalytic hydrogen evolution of polymeric carbon nitride. Nano Energy, 2018, 50, 383-392.	8.2	226
35	The Spatially Oriented Charge Flow and Photocatalysis Mechanism on Internal van der Waals Heterostructures Enhanced g-C <sub>3</sub> N <sub>4</sub> . ACS Catalysis, 2018, 8, 8376-8385.	5.5	219
36	Novel in Situ N-Doped (BiO) <sub>2</sub> CO <sub>3</sub> Hierarchical Microspheres Self-Assembled by Nanosheets as Efficient and Durable Visible Light Driven Photocatalyst. Langmuir, 2012, 28, 766-773.	1.6	218

#	Article	IF	CITATIONS
37	Theoretical and experimental investigation of highly photocatalytic performance of CuInZnS nanoporous structure for removing the NO gas. Journal of Catalysis, 2018, 357, 100-107.	3.1	214
38	2D g-C3N4 for advancement of photo-generated carrier dynamics: Status and challenges. Materials Today, 2020, 41, 270-303.	8.3	214
39	Bi Cocatalyst/Bi <sub>2</sub> MoO <sub>6</sub> Microspheres Nanohybrid with SPR-Promoted Visible-Light Photocatalysis. Journal of Physical Chemistry C, 2016, 120, 11889-11898.	1.5	212
40	Highly Efficient Performance and Conversion Pathway of Photocatalytic NO Oxidation on SrO-Clusters@Amorphous Carbon Nitride. Environmental Science & Technology, 2017, 51, 10682-10690.	4.6	203
41	Bi metal prevents the deactivation of oxygen vacancies in Bi2O2CO3 for stable and efficient photocatalytic NO abatement. Applied Catalysis B: Environmental, 2020, 264, 118545.	10.8	197
42	Unraveling the Mechanisms of Visible Light Photocatalytic NO Purification on Earth-Abundant Insulator-Based Core–Shell Heterojunctions. Environmental Science & Technology, 2018, 52, 1479-1487.	4.6	192
43	Efficient C <sub>3</sub> N <sub>4</sub> /graphene oxide macroscopic aerogel visible-light photocatalyst. Journal of Materials Chemistry A, 2016, 4, 7823-7829.	5.2	185
44	Activation of amorphous Bi2WO6 with synchronous Bi metal and Bi2O3 coupling: Photocatalysis mechanism and reaction pathway. Applied Catalysis B: Environmental, 2018, 232, 340-347.	10.8	179
45	Rational nanostructure design of graphitic carbon nitride for photocatalytic applications. Journal of Materials Chemistry A, 2019, 7, 11584-11612.	5.2	174
46	Steering the interlayer energy barrier and charge flow via bioriented transportation channels in g-C3N4: Enhanced photocatalysis and reaction mechanism. Journal of Catalysis, 2017, 352, 351-360.	3.1	173
47	Facets and defects cooperatively promote visible light plasmonic photocatalysis with Bi nanowires@BiOCl nanosheets. Journal of Catalysis, 2016, 344, 401-410.	3.1	172
48	Visible-Light Photocatalytic Removal of NO in Air over BiOX (X = Cl, Br, I) Single-Crystal Nanoplates Prepared at Room Temperature. Industrial & Engineering Chemistry Research, 2013, 52, 6740-6746.	1.8	170
49	Readily achieving concentration-tunable oxygen vacancies in Bi2O2CO3: Triple-functional role for efficient visible-light photocatalytic redox performance. Applied Catalysis B: Environmental, 2018, 226, 441-450.	10.8	169
50	Role of graphene on the band structure and interfacial interaction of Bi <sub>2</sub> WO <sub>6</sub> /graphene composites with enhanced photocatalytic oxidation of NO. Journal of Materials Chemistry A, 2014, 2, 16623-16631.	5.2	166
51	Facet-dependent interfacial charge separation and transfer in plasmonic photocatalysts. Applied Catalysis B: Environmental, 2018, 226, 269-277.	10.8	166
52	Probing ring-opening pathways for efficient photocatalytic toluene decomposition. Journal of Materials Chemistry A, 2019, 7, 3366-3374.	5.2	166
53	Synergistic integration of Bi metal and phosphate defects on hexagonal and monoclinic BiPO4: Enhanced photocatalysis and reaction mechanism. Applied Catalysis B: Environmental, 2019, 243, 313-321.	10.8	166
54	Monodisperse bismuth nanoparticles decorated graphitic carbon nitride: Enhanced visible-light-response photocatalytic NO removal and reaction pathway. Applied Catalysis B: Environmental, 2017, 205, 532-540.	10.8	162

#	Article	IF	CITATIONS
55	Efficient and Durable Visible Light Photocatalytic Performance of Porous Carbon Nitride Nanosheets for Air Purification. Industrial & Engineering Chemistry Research, 2014, 53, 2318-2330.	1.8	159
56	Directional electron delivery via a vertical channel between g-C <sub>3</sub> N <sub>4</sub> layers promotes photocatalytic efficiency. Journal of Materials Chemistry A, 2017, 5, 9358-9364.	5.2	159
57	Promoting ring-opening efficiency for suppressing toxic intermediates during photocatalytic toluene degradation via surface oxygen vacancies. Science Bulletin, 2019, 64, 669-678.	4.3	159
58	Transformation pathway and toxic intermediates inhibition of photocatalytic NO removal on designed Bi metal@defective Bi2O2SiO3. Applied Catalysis B: Environmental, 2019, 241, 187-195.	10.8	158
59	Rose-like monodisperse bismuth subcarbonate hierarchical hollow microspheres: One-pot template-free fabrication and excellent visible light photocatalytic activity and photochemical stability for NO removal in indoor air. Journal of Hazardous Materials, 2011, 195, 346-354.	6.5	151
60	Fabrication, modification and application of (BiO)2CO3-based photocatalysts: A review. Applied Surface Science, 2016, 365, 314-335.	3.1	147
61	Controlling interfacial contact and exposed facets for enhancing photocatalysis via 2D–2D heterostructures. Chemical Communications, 2015, 51, 8249-8252.	2.2	145
62	Tailoring the rate-determining step in photocatalysis via localized excess electrons for efficient and safe air cleaning. Applied Catalysis B: Environmental, 2018, 239, 187-195.	10.8	145
63	Band structure engineering and efficient charge transport in oxygen substituted g-C3N4 for superior photocatalytic hydrogen evolution. Applied Catalysis B: Environmental, 2018, 230, 115-124.	10.8	143
64	Template-free fabrication and growth mechanism of uniform (BiO)2CO3 hierarchical hollow microspheres with outstanding photocatalytic activities under both UV and visible light irradiation. Journal of Materials Chemistry, 2011, 21, 12428.	6.7	142
65	Reactant activation and photocatalysis mechanisms on Bi-metal@Bi2GeO5 with oxygen vacancies: A combined experimental and theoretical investigation. Chemical Engineering Journal, 2019, 370, 1366-1375.	6.6	141
66	Defective Bi4MoO9/Bi metal core/shell heterostructure: Enhanced visible light photocatalysis and reaction mechanism. Applied Catalysis B: Environmental, 2018, 239, 619-627.	10.8	139
67	Fe-ions modified mesoporous Bi2WO6 nanosheets with high visible light photocatalytic activity. Journal of Colloid and Interface Science, 2012, 369, 373-380.	5.0	138
68	Facile synthesis of surface N-doped Bi2O2CO3: Origin of visible light photocatalytic activity and in situ DRIFTS studies. Journal of Hazardous Materials, 2016, 307, 163-172.	6.5	138
69	Growth of BiOBr nanosheets on C3N4 nanosheets to construct two-dimensional nanojunctions with enhanced photoreactivity for NO removal. Journal of Colloid and Interface Science, 2014, 418, 317-323.	5.0	136
70	Activation of amorphous bismuth oxide via plasmonic Bi metal for efficient visible-light photocatalysis. Journal of Catalysis, 2017, 352, 102-112.	3.1	135
71	Enhancing ROS generation and suppressing toxic intermediate production in photocatalytic NO oxidation on O/Ba co-functionalized amorphous carbon nitride. Applied Catalysis B: Environmental, 2018, 237, 938-946.	10.8	134
72	Three dimensional Z-scheme (BiO) 2 CO 3 /MoS 2 with enhanced visible light photocatalytic NO removal. Applied Catalysis B: Environmental, 2016, 199, 87-95.	10.8	133

#	Article	IF	CITATIONS
73	Visible light induced electron transfer process over nitrogen doped TiO2 nanocrystals prepared by oxidation of titanium nitride. Journal of Hazardous Materials, 2008, 157, 57-63.	6.5	132
74	Band structure and visible light photocatalytic activity of multi-type nitrogen doped TiO2 nanoparticles prepared by thermal decomposition. Journal of Hazardous Materials, 2009, 162, 763-770.	6.5	132
75	KCl-mediated dual electronic channels in layered g-C <sub>3</sub> N <sub>4</sub> for enhanced visible light photocatalytic NO removal. Nanoscale, 2018, 10, 8066-8074.	2.8	126
76	The activation of reactants and intermediates promotes the selective photocatalytic NO conversion on electron-localized Sr-intercalated g-C3N4. Applied Catalysis B: Environmental, 2018, 232, 69-76.	10.8	125
77	Multifunctional g-C 3 N 4 /graphene oxide wrapped sponge monoliths as highly efficient adsorbent and photocatalyst. Applied Catalysis B: Environmental, 2018, 235, 17-25.	10.8	117
78	Simultaneously promoting charge separation and photoabsorption of BiOX (X = Cl, Br) for efficient visible-light photocatalysis and photosensitization by compositing low-cost biochar. Applied Surface Science, 2016, 386, 285-295.	3.1	116
79	Noble metal-free Bi nanoparticles supported on TiO <sub>2</sub> with plasmon-enhanced visible light photocatalytic air purification. Environmental Science: Nano, 2016, 3, 1306-1317.	2.2	114
80	Synchronously Achieving Plasmonic Bi Metal Deposition and I <sup>–</sup> Doping by Utilizing BiOIO <sub>3</sub> as the Self-Sacrificing Template for High-Performance Multifunctional Applications. ACS Applied Materials & Interfaces, 2015, 7, 27925-27933.	4.0	113
81	Synergistic effects of crystal structure and oxygen vacancy on Bi2O3 polymorphs: intermediates activation, photocatalytic reaction efficiency, and conversion pathway. Science Bulletin, 2020, 65, 467-476.	4.3	108
82	Electrocatalytic hydrodechlorination of 2,4-dichlorophenol over palladium nanoparticles and its pH-mediated tug-of-war with hydrogen evolution. Chemical Engineering Journal, 2018, 348, 26-34.	6.6	104
83	Mechanism of visible light photocatalytic NO <sub>x</sub> oxidation with plasmonic Bi cocatalyst-enhanced (BiO) <sub>2</sub> CO <sub>3</sub> hierarchical microspheres. Physical Chemistry Chemical Physics, 2015, 17, 10383-10390.	1.3	103
84	In situ synthesis of a C-doped (BiO) <sub>2</sub> CO <sub>3</sub> hierarchical self-assembly effectively promoting visible light photocatalysis. Journal of Materials Chemistry A, 2015, 3, 6118-6127.	5.2	103
85	Directional electron delivery and enhanced reactants activation enable efficient photocatalytic air purification on amorphous carbon nitride co-functionalized with O/La. Applied Catalysis B: Environmental, 2019, 242, 19-30.	10.8	103
86	Improving g-C3N4 photocatalysis for NOx removal by Ag nanoparticles decoration. Applied Surface Science, 2015, 358, 356-362.	3.1	101
87	New insights into how Pd nanoparticles influence the photocatalytic oxidation and reduction ability of g-C <sub>3</sub> N <sub>4</sub> nanosheets. Catalysis Science and Technology, 2016, 6, 6448-6458.	2.1	101
88	In situ FT-IR investigation on the reaction mechanism of visible light photocatalytic NO oxidation with defective g-C3N4. Science Bulletin, 2018, 63, 117-125.	4.3	101
89	Boosting Visible-Light-Driven Photo-oxidation of BiOCl by Promoted Charge Separation via Vacancy Engineering. ACS Sustainable Chemistry and Engineering, 2019, 7, 3010-3017.	3.2	101
90	Highly Efficient Bi <sub>2</sub> O <sub>2</sub> CO <sub>3</sub> Single-Crystal Lamellas with Dominantly Exposed {001} Facets. Crystal Growth and Design, 2015, 15, 534-537.	1.4	99

#	Article	IF	CITATIONS
91	Unraveling the mechanism of binary channel reactions in photocatalytic formaldehyde decomposition for promoted mineralization. Applied Catalysis B: Environmental, 2020, 260, 118130.	10.8	99
92	In situ decoration of plasmonic Ag nanocrystals on the surface of (BiO) <sub>2</sub> CO <sub>3</sub> hierarchical microspheres for enhanced visible light photocatalysis. Dalton Transactions, 2014, 43, 9468-9480.	1.6	98
93	Bi metal sphere/graphene oxide nanohybrids with enhanced direct plasmonic photocatalysis. Applied Catalysis B: Environmental, 2017, 214, 148-157.	10.8	98
94	Synergistic Photocatalytic Decomposition of a Volatile Organic Compound Mixture: High Efficiency, Reaction Mechanism, and Long-Term Stability. ACS Catalysis, 2020, 10, 7230-7239.	5.5	98
95	Ti3C2 MXene modified g-C3N4 with enhanced visible-light photocatalytic performance for NO purification. Journal of Colloid and Interface Science, 2020, 575, 443-451.	5.0	98
96	A general method for type I and type II g-C <sub>3</sub> N <sub>4</sub> /g-C <sub>3</sub> N <sub>4</sub> metal-free isotype heterostructures with enhanced visible light photocatalysis. New Journal of Chemistry, 2015, 39, 4737-4744.	1.4	95
97	Facile synthesis of organic–inorganic layered nanojunctions of g-C <sub>3</sub> N <sub>4</sub> /(BiO) <sub>2</sub> CO <sub>3</sub> as efficient visible light photocatalyst. Dalton Transactions, 2014, 43, 12026-12036.	1.6	92
98	Enhancing the photocatalytic activity of bulk g-C3N4 by introducing mesoporous structure and hybridizing with graphene. Journal of Colloid and Interface Science, 2014, 436, 29-36.	5.0	92
99	Bismuth spheres assembled on graphene oxide: Directional charge transfer enhances plasmonic photocatalysis and in situ DRIFTS studies. Applied Catalysis B: Environmental, 2018, 221, 482-489.	10.8	92
100	Template synthesis of carbon self-doped g-C <sub>3</sub> N <sub>4</sub> with enhanced visible to near-infrared absorption and photocatalytic performance. RSC Advances, 2015, 5, 39549-39556.	1.7	91
101	Easily and Synchronously Ameliorating Charge Separation and Band Energy Level in Porous g-C <sub>3</sub> N <sub>4</sub> for Boosting Photooxidation and Photoreduction Ability. Journal of Physical Chemistry C, 2016, 120, 10381-10389.	1.5	91
102	Cu supported on polymeric carbon nitride for selective CO <sub>2</sub> reduction into CH <sub>4</sub> : a combined kinetics and thermodynamics investigation. Journal of Materials Chemistry A, 2019, 7, 17014-17021.	5.2	90
103	Plasmonic Bi metal as cocatalyst and photocatalyst: The case of Bi/(BiO) 2 CO 3 and Bi particles. Journal of Colloid and Interface Science, 2017, 485, 1-10.	5.0	89
104	The pivotal roles of spatially separated charge localization centers on the molecules activation and photocatalysis mechanism. Applied Catalysis B: Environmental, 2020, 262, 118251.	10.8	89
105	Marked enhancement of photocatalytic activity and photochemical stability of N–doped TiO2 nanocrystals by Fe3+/Fe2+ surface modification. Journal of Colloid and Interface Science, 2010, 343, 200-208.	5.0	88
106	From semiconductors to semimetals: bismuth as a photocatalyst for NO oxidation in air. Journal of Materials Chemistry A, 2014, 2, 11065-11072.	5.2	88
107	The pivotal effects of oxygen vacancy on Bi2MoO6: Promoted visible light photocatalytic activity and reaction mechanism. Chinese Journal of Catalysis, 2019, 40, 647-655.	6.9	86
108	Rapid Self-Decomposition of g-C <sub>3</sub> N <sub>4</sub> During Gas–Solid Photocatalytic CO <sub>2</sub> Reduction and Its Effects on Performance Assessment. ACS Catalysis, 2022, 12, 4560-4570.	5.5	86

#	Article	IF	CITATIONS
109	The importance of intermediates ring-opening in preventing photocatalyst deactivation during toluene decomposition. Applied Catalysis B: Environmental, 2020, 272, 118977.	10.8	84
110	Enhanced visible light photocatalytic activity of novel Pt/C-doped TiO2/PtCl4 three-component nanojunction system for degradation of toluene in air. Journal of Hazardous Materials, 2011, 187, 509-516.	6.5	83
111	(NH4)2CO3 mediated hydrothermal synthesis of N-doped (BiO)2CO3 hollow nanoplates microspheres as high-performance and durable visible light photocatalyst for air cleaning. Chemical Engineering Journal, 2013, 214, 198-207.	6.6	83
112	The activation of oxygen through oxygen vacancies in BiOCl/PPy to inhibit toxic intermediates and enhance the activity of photocatalytic nitric oxide removal. Nanoscale, 2019, 11, 6360-6367.	2.8	83
113	Theoretical design and experimental investigation on highly selective Pd particles decorated C3N4 for safe photocatalytic NO purification. Journal of Hazardous Materials, 2020, 392, 122357.	6.5	81
114	One-pot template-free synthesis, growth mechanism and enhanced photocatalytic activity of monodisperse (BiO)2CO3 hierarchical hollow microspheres self-assembled with single-crystalline nanosheets. CrystEngComm, 2012, 14, 3534.	1.3	79
115	Biâ€based photocatalysts for <scp>lightâ€driven</scp> environmental and energy applications: Structural tuning, reaction mechanisms, and challenges. EcoMat, 2020, 2, e12047.	6.8	79
116	Synergistic integration of metallic Bi and defects on BiOI: Enhanced photocatalytic NO removal and conversion pathway. Chinese Journal of Catalysis, 2019, 40, 826-836.	6.9	78
117	Mechanisms of Interfacial Charge Transfer and Photocatalytic NO Oxidation on BiOBr/SnO <sub>2</sub> p–n Heterojunctions. ACS Applied Materials & Interfaces, 2020, 12, 43741-43749.	4.0	77
118	Bi quantum dots implanted 2D C-doped BiOCl nanosheets: Enhanced visible light photocatalysis efficiency and reaction pathway. Chinese Journal of Catalysis, 2020, 41, 1430-1438.	6.9	77
119	Bismuth nanoparticles and oxygen vacancies synergistically attired Zn2SnO4 with optimized visible-light-active performance. Nano Energy, 2021, 80, 105415.	8.2	77
120	Monolayer Epitaxial Heterostructures for Selective Visibleâ€Lightâ€Driven Photocatalytic NO Oxidation. Advanced Functional Materials, 2019, 29, 1808084.	7.8	76
121	Oxygen vacancy engineering of self-doped SnO <sub>2â^'x</sub> nanocrystals for ultrasensitive NO <sub>2</sub> detection. Journal of Materials Chemistry C, 2020, 8, 487-494.	2.7	76
122	Surface oxygen-vacancy induced photocatalytic activity of La(OH) <sub>3</sub> nanorods prepared by a fast and scalable method. Physical Chemistry Chemical Physics, 2015, 17, 16058-16066.	1.3	75
123	Three-dimensional MoS 2 /reduced graphene oxide aerogel as a macroscopic visible-light photocatalyst. Chinese Journal of Catalysis, 2017, 38, 313-320.	6.9	75
124	Synergistic photo-thermal catalytic NO purification of MnO /g-C3N4: Enhanced performance and reaction mechanism. Chinese Journal of Catalysis, 2018, 39, 619-629.	6.9	75
125	Efficient visible light photocatalytic oxidation of NO in air with band-gap tailored (BiO)2CO3–BiOI solid solutions. Chemical Engineering Journal, 2014, 255, 650-658.	6.6	74
126	Achieving tunable photocatalytic activity enhancement by elaborately engineering composition-adjustable polynary heterojunctions photocatalysts. Applied Catalysis B: Environmental, 2016, 194, 62-73.	10.8	73

#	Article	IF	CITATIONS
127	2D BiOCl/Bi 12 O 17 Cl 2 nanojunction: Enhanced visible light photocatalytic NO removal and in situ DRIFTS investigation. Applied Surface Science, 2018, 430, 571-577.	3.1	73
128	Photocatalytic NO oxidation on N-doped TiO2/g-C3N4 heterojunction: Enhanced efficiency, mechanism and reaction pathway. Applied Surface Science, 2018, 458, 77-85.	3.1	73
129	Highly enhanced visible-light photocatalytic NO x purification and conversion pathway on self-structurally modified g-C 3 N 4 nanosheets. Science Bulletin, 2018, 63, 609-620.	4.3	72
130	Ba-vacancy induces semiconductor-like photocatalysis on insulator BaSO4. Applied Catalysis B: Environmental, 2019, 253, 293-299.	10.8	72
131	Mass-Controlled Direct Synthesis of Graphene-like Carbon Nitride Nanosheets with Exceptional High Visible Light Activity. Less is Better. Scientific Reports, 2015, 5, 14643.	1.6	71
132	New insights into how RGO influences the photocatalytic performance of BiOIO3/RGO nanocomposites under visible and UV irradiation. Journal of Colloid and Interface Science, 2015, 447, 16-24.	5.0	71
133	A new strategy for utilization of NIR from solar energy—Promotion effect generated from photothermal effect of Fe3O4@SiO2 for photocatalytic oxidation of NO. Applied Catalysis B: Environmental, 2017, 204, 584-592.	10.8	70
134	SnO2 quantum dots anchored on g-C3N4 for enhanced visible-light photocatalytic removal of NO and toxic NO2 inhibition. Applied Surface Science, 2019, 496, 143630.	3.1	68
135	Tuning the reaction pathway of photocatalytic NO oxidation process to control the secondary pollution on monodisperse Au nanoparticles@g-C3N4. Chemical Engineering Journal, 2019, 378, 122184.	6.6	68
136	Synergistic integration of thermocatalysis and photocatalysis on black defective (BiO) <sub>2</sub> CO <sub>3</sub> microspheres. Journal of Materials Chemistry A, 2015, 3, 18466-18474.	5.2	67
137	Solvent-assisted synthesis of porous g-C 3 N 4 with efficient visible-light photocatalytic performance for NO removal. Chinese Journal of Catalysis, 2017, 38, 372-378.	6.9	67
138	Effects of Morphology and Crystallinity on the Photocatalytic Activity of (BiO) <sub>2</sub> CO <sub>3</sub> Nano/microstructures. Industrial & Engineering Chemistry Research, 2014, 53, 15002-15011.	1.8	66
139	Interlayer-I-doped BiOIO <sub>3</sub> nanoplates with an optimized electronic structure for efficient visible light photocatalysis. Chemical Communications, 2016, 52, 8243-8246.	2.2	66
140	Efficient visible light photocatalytic oxidation of NO with hierarchical nanostructured 3D flower-like BiOClxBr1â^'x solid solutions. Journal of Alloys and Compounds, 2016, 671, 318-327.	2.8	66
141	Controlled synthesis, growth mechanism and highly efficient solar photocatalysis of nitrogen-doped bismuth subcarbonate hierarchical nanosheets architectures. Dalton Transactions, 2012, 41, 8270.	1.6	65
142	Pivotal roles of artificial oxygen vacancies in enhancing photocatalytic activity and selectivity on Bi2O2CO3 nanosheets. Chinese Journal of Catalysis, 2019, 40, 620-630.	6.9	65
143	Single Precursor Mediated-Synthesis of Bi Semimetal Deposited N-Doped (BiO) <sub>2</sub> CO <sub>3</sub> Superstructures for Highly Promoted Photocatalysis. ACS Sustainable Chemistry and Engineering, 2016, 4, 2969-2979.	3.2	64
144	N-Doped Bi <sub>2</sub> O <sub>2</sub> CO <sub>3</sub> /Graphene Quantum Dot Composite Photocatalyst: Enhanced Visible-Light Photocatalytic NO Oxidation and In Situ DRIFTS Studies. Journal of Physical Chemistry C, 2017, 121, 12168-12177.	1.5	64

#	Article	IF	CITATIONS
145	A Bi/BiOI/(BiO)2CO3 heterostructure for enhanced photocatalytic NO removal under visible light. Chinese Journal of Catalysis, 2019, 40, 362-370.	6.9	63
146	Tailoring Active Sites via Synergy between Graphitic and Pyridinic N for Enhanced Catalytic Efficiency of a Carbocatalyst. ACS Applied Materials & Interfaces, 2017, 9, 19861-19869.	4.0	62
147	Uncovering the synergy between Mn substitution and O vacancy in ZnAl-LDH photocatalyst for efficient toluene removal. Applied Catalysis B: Environmental, 2021, 296, 120376.	10.8	62
148	Atomic interfacial structure and charge transfer mechanism on in-situ formed BiOI/Bi2O2SO4 p–n heterojunctions with highly promoted photocatalysis. Applied Catalysis B: Environmental, 2021, 297, 120492.	10.8	62
149	Light-Induced Generation and Regeneration of Oxygen Vacancies in BiSbO <sub>4</sub> for Sustainable Visible Light Photocatalysis. ACS Applied Materials & Interfaces, 2019, 11, 47984-47991.	4.0	61
150	Efficient and stable photocatalytic NO removal on C self-doped g-C <sub>3</sub> N <sub>4</sub> : electronic structure and reaction mechanism. Catalysis Science and Technology, 2018, 8, 3387-3394.	2.1	60
151	BaWO4/g-C3N4 heterostructure with excellent bifunctional photocatalytic performance. Chemical Engineering Journal, 2020, 385, 123833.	6.6	60
152	C3N4 with engineered three coordinated (N3C) nitrogen vacancy boosts the production of 1O2 for Efficient and stable NO photo-oxidation. Chemical Engineering Journal, 2020, 389, 124421.	6.6	60
153	Iodide surface decoration: a facile and efficacious approach to modulating the band energy level of semiconductors for high-performance visible-light photocatalysis. Chemical Communications, 2016, 52, 354-357.	2.2	59
154	Nature-inspired CaCO3 loading TiO2 composites for efficient and durable photocatalytic mineralization of gaseous toluene. Science Bulletin, 2020, 65, 1626-1634.	4.3	59
155	Carbonate-intercalated defective bismuth tungstate for efficiently photocatalytic NO removal and promotion mechanism study. Applied Catalysis B: Environmental, 2019, 254, 206-213.	10.8	58
156	Single-Atom Ru-Implanted Metal–Organic Framework/MnO <sub>2</sub> for the Highly Selective Oxidation of NO <sub><i>x</i></sub> by Plasma Activation. ACS Catalysis, 2020, 10, 10185-10196.	5.5	58
157	Improving visible-light-driven photocatalytic NO oxidation over BiOBr nanoplates through tunable oxygen vacancies. Chinese Journal of Catalysis, 2018, 39, 779-789.	6.9	57
158	Unveiling the unconventional roles of methyl number on the ring-opening barrier in photocatalytic decomposition of benzene, toluene and o-xylene. Applied Catalysis B: Environmental, 2020, 278, 119318.	10.8	57
159	An anion-exchange strategy for 3D hierarchical (BiO) <sub>2</sub> CO <sub>3</sub> /amorphous Bi <sub>2</sub> S <sub>3</sub> heterostructures with increased solar absorption and enhanced visible light photocatalysis. RSC Advances, 2015, 5, 11714-11723.	1.7	56
160	Facile synthesis of Bi12O17Br2 and Bi4O5Br2 nanosheets: In situ DRIFTS investigation of photocatalytic NO oxidation conversion pathway. Chinese Journal of Catalysis, 2017, 38, 2030-2038.	6.9	56
161	One-step preparation of a novel SrCO <sub>3</sub> /g-C <sub>3</sub> N <sub>4</sub> nano-composite and its application in selective adsorption of crystal violet. RSC Advances, 2018, 8, 6315-6325.	1.7	56
162	Ag/AgCl nanoparticles assembled on BiOCl/Bi12O17Cl2 nanosheets: Enhanced plasmonic visible light photocatalysis and in situ DRIFTS investigation. Applied Surface Science, 2018, 455, 236-243.	3.1	56

#	Article	IF	CITATIONS
163	Enhancement of the visible light photocatalytic performance of C-doped TiO2 by loading with V2O5. Catalysis Communications, 2009, 11, 82-86.	1.6	55
164	Hydrothermal formation of N-doped (BiO)2CO3 honeycomb-like microspheres photocatalysts with bismuth citrate and dicyandiamide as precursors. Journal of Colloid and Interface Science, 2013, 408, 33-42.	5.0	55
165	Ternary Ag/AgCl/BiOIO3 composites for enhanced visible-light-driven photocatalysis. Chinese Journal of Catalysis, 2015, 36, 2155-2163.	6.9	54
166	Integrating the merits of two-dimensional structure and heteroatom modification into semiconductor photocatalyst to boost NO removal. Chemical Engineering Journal, 2019, 370, 944-951.	6.6	54
167	Activating earth-abundant insulator BaSO4 for visible-light induced degradation of tetracycline. Applied Catalysis B: Environmental, 2022, 307, 121182.	10.8	54
168	Heterostructured BiOI@La(OH) 3 nanorods with enhanced visible light photocatalytic NO removal. Chinese Journal of Catalysis, 2017, 38, 217-226.	6.9	53
169	Visible light induced electron transfer from a semiconductor to an insulator enables efficient photocatalytic activity on insulator-based heterojunctions. Nanoscale, 2018, 10, 15513-15520.	2.8	53
170	Ultrathin Two-Dimensional Bi-Based photocatalysts: Synthetic strategies, surface defects, and reaction mechanisms. Chemical Engineering Journal, 2021, 417, 129305.	6.6	52
171	In situ loading of MoO3 clusters on ultrathin Bi2MoO6 nanosheets for synergistically enhanced photocatalytic NO abatement. Applied Catalysis B: Environmental, 2021, 292, 120159.	10.8	51
172	Pt quantum dots deposited on N-doped (BiO) <sub>2</sub> CO <sub>3</sub> : enhanced visible light photocatalytic NO removal and reaction pathway. Catalysis Science and Technology, 2017, 7, 1324-1332.	2.1	50
173	Insights into Dynamic Surface Bromide Sites in Bi <sub>4</sub> O <sub>5</sub> Br <sub>2</sub> for Sustainable N <sub>2</sub> Photofixation. Angewandte Chemie - International Edition, 2022, 61, .	7.2	50
174	Mesoporous Ni-Doped δ-Bi <sub>2</sub> O <sub>3</sub> Microspheres for Enhanced Solar-Driven Photocatalysis: A Combined Experimental and Theoretical Investigation. Journal of Physical Chemistry C, 2017, 121, 9394-9401.	1.5	49
175	Facet-dependent photocatalytic NO conversion pathways predetermined by adsorption activation patterns. Nanoscale, 2019, 11, 2366-2373.	2.8	49
176	Synergistic effect of manganese dioxide and diatomite for fast decolorization and high removal capacity of methyl orange. Journal of Colloid and Interface Science, 2016, 484, 1-9.	5.0	48
177	Efficient visible light photocatalytic NOx removal with cationic Ag clusters-grafted (BiO)2CO3 hierarchical superstructures. Journal of Hazardous Materials, 2017, 322, 223-232.	6.5	48
178	Exploring the photocatalysis mechanism on insulators. Applied Catalysis B: Environmental, 2017, 219, 450-458.	10.8	48
179	Photocatalytic Platforms for Removal of Ammonia from Gaseous and Aqueous Matrixes: Status and Challenges. ACS Catalysis, 2020, 10, 8683-8716.	5.5	48
180	The high selectivity for benzoic acid formation on Ca2Sb2O7 enables efficient and stable toluene mineralization. Applied Catalysis B: Environmental, 2020, 271, 118948.	10.8	48

#	Article	IF	CITATIONS
181	Enhanced extrinsic absorption promotes the visible light photocatalytic activity of wide band-gap (BiO) <sub>2</sub> CO <sub>3</sub> hierarchical structure. RSC Advances, 2014, 4, 56307-56312.	1.7	47
182	High visible-light photocatalytic performance of stable lead-free Cs2AgBiBr6 double perovskite nanocrystals. Journal of Catalysis, 2021, 397, 27-35.	3.1	47
183	Facile Synthesis of Flower-like (BiO)2CO3@MnO2 and Bi2O3@MnO2 Nanocomposites for Supercapacitors. Electrochimica Acta, 2015, 168, 97-103.	2.6	46
184	Humidity-Independent Photocatalytic Toluene Mineralization Benefits from the Utilization of Edge Hydroxyls in Layered Double Hydroxides (LDHs): A Combined Operando and Theoretical Investigation. ACS Catalysis, 2021, 11, 8132-8139.	5.5	46
185	Growth mechanism and photocatalytic activity of self-organized N-doped (BiO) <sub>2</sub> CO <sub>3</sub> hierarchical nanosheet microspheres from bismuth citrate and urea. Dalton Transactions, 2014, 43, 6631-6642.	1.6	45
186	Threeâ€inâ€One Oxygen Vacancies: Whole Visibleâ€Spectrum Absorption, Efficient Charge Separation, and Surface Site Activation for Robust CO <sub>2</sub> Photoreduction. Angewandte Chemie, 2019, 131, 3920-3924.	1.6	45
187	Dual redox couples Ag/Ag+ and lâ^'/(IO3)â^' self-sacrificed transformation for realizing multiplex hierarchical architectures with universally powerful photocatalytic performance. Applied Catalysis B: Environmental, 2017, 200, 620-632.	10.8	44
188	Facile synthesis of CeO2/g-C3N4 nanocomposites with significantly improved visible-light photocatalytic activity for hydrogen evolution. International Journal of Hydrogen Energy, 2019, 44, 16154-16163.	3.8	43
189	La-doping induced localized excess electrons on (BiO)2CO3 for efficient photocatalytic NO removal and toxic intermediates suppression. Journal of Hazardous Materials, 2020, 400, 123174.	6.5	43
190	Oxygen vacancies on the BiOCl surface promoted photocatalytic complete NO oxidation via superoxide radicals. Chinese Chemical Letters, 2020, 31, 2737-2741.	4.8	43
191	Enhanced plasmonic photocatalysis by SiO 2 @Bi microspheres with hot-electron transportation channels via Bi–O–Si linkages. Chinese Journal of Catalysis, 2017, 38, 1174-1183.	6.9	42
192	Enhanced photocatalytic NO removal with the superior selectivity for NO2â^'/NO3â^' species of Bi12GeO20-based composites via a ball-milling treatment: Synergetic effect of surface oxygen vacancies and n-p heterojunctions. Composites Part B: Engineering, 2022, 231, 109600.	5.9	42
193	Simultaneous introduction of oxygen vacancies and Bi metal onto the {001} facet of Bi <sub>3</sub> O <sub>4</sub> Cl woven nanobelts for synergistically enhanced photocatalysis. Nanoscale, 2018, 10, 16928-16934.	2.8	41
194	Efficient α-MnO2 with (2 1 0) facet exposed for catalytic oxidation of toluene at low temperature: A combined in-situ DRIFTS and theoretical investigation. Chemosphere, 2021, 263, 128103.	4.2	41
195	Synthesis of BiOBr–graphene and BiOBr–graphene oxide nanocomposites with enhanced visible light photocatalytic performance. Ceramics International, 2014, 40, 9003-9008.	2.3	40
196	A self-sacrifice template route to iodine modified BiOIO <sub>3</sub> : band gap engineering and highly boosted visible-light active photoreactivity. Physical Chemistry Chemical Physics, 2016, 18, 7851-7859.	1.3	40
197	Photocatalytic removal of NO by intercalated carbon nitride: The effect of group IIA element ions. Applied Catalysis B: Environmental, 2020, 273, 119007.	10.8	40
198	Facile construction of Bi2Mo3O12@Bi2O2CO3 heterojunctions for enhanced photocatalytic efficiency toward NO removal and study of the conversion process. Chinese Journal of Catalysis, 2020, 41, 268-275.	6.9	39

#	Article	IF	CITATIONS
199	Interfacial activation of reactants and intermediates on CaSO4 insulator-based heterostructure for efficient photocatalytic NO removal. Chemical Engineering Journal, 2020, 390, 124609.	6.6	39
200	Capture of atmospheric CO2 into (BiO)2CO3/graphene or graphene oxide nanocomposites with enhanced photocatalytic performance. Applied Surface Science, 2015, 358, 75-83.	3.1	38
201	Mechanistic understanding of ternary Ag/AgCl@La(OH) <sub>3</sub> nanorods as novel visible light plasmonic photocatalysts. Catalysis Science and Technology, 2016, 6, 5003-5010.	2.1	37
202	Graphene oxide mediated co-generation of C-doping and oxygen defects in Bi <sub>2</sub> WO <sub>6</sub> nanosheets: a combined DRIFTS and DFT investigation. Nanoscale, 2019, 11, 20562-20570.	2.8	37
203	Zn-doping mediated formation of oxygen vacancies in SnO2 with unique electronic structure for efficient and stable photocatalytic toluene degradation. Chinese Journal of Catalysis, 2021, 42, 1195-1204.	6.9	37
204	Fe( <scp>iii</scp> ) cluster-grafted (BiO) <sub>2</sub> CO <sub>3</sub> superstructures: in situ DRIFTS investigation on IFCT-enhanced visible light photocatalytic NO oxidation. Environmental Science: Nano, 2017, 4, 604-612.	2.2	36
205	High-efficiency photocatalytic decomposition of toluene over defective InOOH: Promotive role of oxygen vacancies in ring opening process. Chemical Engineering Journal, 2021, 413, 127389.	6.6	36
206	Enhanced Visible Light Photocatalytic Activity ofV2O5Cluster Modified N-DopedTiO2for Degradation of Toluene in Air. International Journal of Photoenergy, 2012, 2012, 1-10.	1.4	35
207	Selective breakage of C H bonds in the key oxidation intermediates of gaseous formaldehyde on self-doped CaSn(OH)6 cubes for safe and efficient photocatalysis. Applied Catalysis B: Environmental, 2020, 277, 119214.	10.8	35
208	Controlled deposition of Au on (BiO) <sub>2</sub> CO <sub>3</sub> microspheres: the size and content of Au nanoparticles matter. Dalton Transactions, 2015, 44, 8805-8811.	1.6	34
209	Promoted reactants activation and charge separation leading to efficient photocatalytic activity on phosphate/potassium co-functionalized carbon nitride. Chinese Chemical Letters, 2019, 30, 875-880.	4.8	34
210	Grand Challenges for Catalytic Remediation in Environmental and Energy Applications Toward a Cleaner and Sustainable Future. Frontiers in Environmental Chemistry, 2020, 1, .	0.7	34
211	Synthesis of mesoporous polymeric carbon nitride exhibiting enhanced and durable visible light photocatalytic performance. Science Bulletin, 2014, 59, 688-698.	1.7	33
212	BiOBr with oxygen vacancies capture 0D black phosphorus quantum dots for high efficient photocatalytic ofloxacin degradation. Applied Surface Science, 2022, 593, 153422.	3.1	33
213	The Multiple Effects of Precursors on the Properties of Polymeric Carbon Nitride. International Journal of Photoenergy, 2013, 2013, 1-9.	1.4	32
214	Ternary Ag/AgCl-(BiO) 2 CO 3 composites as high-performance visible-light plasmonic photocatalysts. Catalysis Today, 2017, 284, 67-76.	2.2	32
215	SrTiO3/BiOI heterostructure: Interfacial charge separation, enhanced photocatalytic activity, and reaction mechanism. Chinese Journal of Catalysis, 2020, 41, 710-718.	6.9	32
216	Heterojunction interface of zinc oxide and zinc sulfide promoting reactive molecules activation and carrier separation toward efficient photocatalysis. Journal of Colloid and Interface Science, 2021, 588, 826-837.	5.0	32

#	Article	IF	CITATIONS
217	Photochemical Transformation Pathways of Nitrates from Photocatalytic NOx Oxidation: Implications for Controlling Secondary Pollutants. Environmental Science and Technology Letters, 2021, 8, 873-877.	3.9	32
218	Enhanced Photocatalytic VOCs Mineralization via Special Ga-O-H Charge Transfer Channel in α-Ga <sub>2</sub> O <sub>3</sub> /MgAl-LDH Heterojunction. ACS ES&T Engineering, 2021, 1, 501-511.	3.7	32
219	Optimizing the Electronic Structure of BiOBr Nanosheets via Combined Ba Doping and Oxygen Vacancies for Promoted Photocatalysis. Journal of Physical Chemistry C, 2021, 125, 8597-8605.	1.5	31
220	Anion intercalated layered-double-hydroxide structure for efficient photocatalytic NO remove. Green Energy and Environment, 2019, 4, 270-277.	4.7	30
221	Insights for optimum cation defects in photocatalysis: A case study of hematite nanostructures. Applied Catalysis B: Environmental, 2020, 264, 118506.	10.8	30
222	Efficient photocatalytic toluene degradation over heterojunction of GQDs@BiOCl ultrathin nanosheets with selective benzoic acid activation. Journal of Hazardous Materials, 2021, 420, 126577.	6.5	30
223	Novel CaCO3/g-C3N4 composites with enhanced charge separation and photocatalytic activity. Journal of Saudi Chemical Society, 2019, 23, 1109-1118.	2.4	29
224	An atomic insight into BiOBr/La <sub>2</sub> Ti <sub>2</sub> O <sub>7</sub> p–n heterojunctions: interfacial charge transfer pathway and photocatalysis mechanism. Catalysis Science and Technology, 2020, 10, 826-834.	2.1	28
225	Motivated surface reaction thermodynamics on the bismuth oxyhalides with lattice strain for enhanced photocatalytic NO oxidation. Applied Catalysis B: Environmental, 2021, 284, 119694.	10.8	28
226	Photocatalytic reaction mechanisms at a gas–solid interface for typical air pollutant decomposition. Journal of Materials Chemistry A, 2021, 9, 20184-20210.	5.2	28
227	Hydrothermal fabrication of N-doped (BiO)2CO3: Structural and morphological influence on the visible light photocatalytic activity. Applied Surface Science, 2014, 319, 256-264.	3.1	27
228	Inhibition of the toxic byproduct during photocatalytic NO oxidation via La doping in ZnO. Chinese Chemical Letters, 2020, 31, 751-754.	4.8	27
229	Lightâ€Induced Dynamic Stability of Oxygen Vacancies in BiSbO <sub>4</sub> for Efficient Photocatalytic Formaldehyde Degradation. Energy and Environmental Materials, 2022, 5, 305-312.	7.3	27
230	Optimizing the metal-support interactions at the Pd-polymer carbon nitride Mott-Schottky heterojunction interface for an enhanced electrocatalytic hydrodechlorination reaction. Journal of Hazardous Materials, 2021, 411, 125119.	6.5	27
231	Porous Mn-doped Co3O4 nanosheets: Gas sensing performance and interfacial mechanism investigation with In situ DRIFTS. Sensors and Actuators B: Chemical, 2022, 353, 131155.	4.0	27
232	Ammonia induced formation of N-doped (BiO)2CO3 hierarchical microspheres: the effect of hydrothermal temperature on the morphology and photocatalytic activity. CrystEngComm, 2013, 15, 10522.	1.3	26
233	Synergetic effect of BiOCl/Bi12O17Cl2 and MoS2: in situ DRIFTS investigation on photocatalytic NO oxidation pathway. Rare Metals, 2019, 38, 437-445.	3.6	26
234	The rapid synthesis of photocatalytic (BiO) <sub>2</sub> CO <sub>3</sub> single-crystal nanosheets via an eco-friendly approach. CrystEngComm, 2014, 16, 3592-3604.	1.3	25

#	Article	IF	CITATIONS
235	In situ growth of Au nanoparticles on 3D Bi <sub>2</sub> O <sub>2</sub> CO <sub>3</sub> for surface plasmon enhanced visible light photocatalysis. New Journal of Chemistry, 2015, 39, 8446-8453.	1.4	25
236	Facile synthesis of in situ phosphorus-doped g-C <sub>3</sub> N <sub>4</sub> with enhanced visible light photocatalytic property for NO purification. RSC Advances, 2016, 6, 88085-88089.	1.7	24
237	Enhanced plasmonic photocatalytic disinfection on noble-metal-free bismuth nanospheres/graphene nanocomposites. Catalysis Science and Technology, 2018, 8, 4600-4603.	2.1	24
238	Carbonate doped Bi2MoO6 hierarchical nanostructure with enhanced transformation of active radicals for efficient photocatalytic removal of NO. Journal of Colloid and Interface Science, 2019, 557, 816-824.	5.0	24
239	Oxygen activation of noble-metal-free g-C3N4/α-Ni(OH)2 to control the toxic byproduct of photocatalytic nitric oxide removal. Chemical Engineering Journal, 2020, 382, 123029.	6.6	24
240	Highly enhanced photocatalytic toluene degradation and in situ FT-IR investigation on designed Sn-doped BiOCl nanosheets. Applied Surface Science, 2022, 578, 152002.	3.1	24
241	Reheat treatment under vacuum induces pre-calcined α-MnO2 with oxygen vacancy as efficient catalysts for toluene oxidation. Chemosphere, 2022, 289, 133081.	4.2	24
242	In situ DRIFT investigation on the photocatalytic NO oxidation mechanism with thermally exfoliated porous g-C <sub>3</sub> N <sub>4</sub> nanosheets. RSC Advances, 2017, 7, 19280-19287.	1.7	23
243	Promote reactants activation and key intermediates formation for facilitated toluene photodecomposition via Ba active sites construction. Applied Catalysis B: Environmental, 2021, 297, 120489.	10.8	23
244	Non-noble metal plasmonic photocatalysis in semimetal bismuth films for photocatalytic NO oxidation. Physical Chemistry Chemical Physics, 2017, 19, 25610-25616.	1.3	22
245	Surface Hydrogen Atoms Promote Oxygen Activation for Solar Light-Driven NO Oxidization over Monolithic α-Ni(OH) <sub>2</sub> /Ni Foam. Environmental Science & Technology, 2020, 54, 16221-16230.	4.6	22
246	Controlled hydrogenation into defective interlayer bismuth oxychloride via vacancy engineering. Communications Chemistry, 2020, 3, .	2.0	22
247	Highly efficient photocatalytic NO removal and in situ DRIFTS investigation on SrSn(OH)6. Chinese Chemical Letters, 2022, 33, 1259-1262.	4.8	22
248	A Cost-Effective Solid-State Approach to Synthesize g-C <sub>3</sub> N <sub>4</sub> Coated TiO <sub>2</sub> Nanocomposites with Enhanced Visible Light Photocatalytic Activity. International Journal of Photoenergy, 2013, 2013, 1-7.	1.4	21
249	Growth of g-C <sub>3</sub> N <sub>4</sub> Layer on Commercial TiO <sub>2</sub> for Enhanced Visible Light Photocatalytic Activity. Journal of Nanomaterials, 2014, 2014, 1-8.	1.5	21
250	Simultaneous Pd2+ doping and Pd metal deposition on (BiO)2CO3 microspheres for enhanced and stable visible light photocatalysis. Applied Catalysis A: General, 2016, 510, 161-170.	2.2	21
251	Tuning the Active Sites of Atomically Thin Defective Bi <sub>12</sub> O <sub>17</sub> Cl <sub>2</sub> via Incorporation of Subnanometer Clusters. ACS Applied Materials & Interfaces, 2021, 13, 9216-9223.	4.0	21
252	Identification of deactivation-resistant origin of In(OH)3 for efficient and durable photodegradation of benzene, toluene and their mixtures. Journal of Hazardous Materials, 2021, 416, 126208.	6.5	21

#	Article	IF	CITATIONS
253	Thermocatalytic oxidation of gaseous benzene by a titanium dioxide supported platinum catalyst. Chemical Engineering Journal, 2022, 428, 131090.	6.6	21
254	Sulfur-doping synchronously ameliorating band energy structure and charge separation achieving decent visible-light photocatalysis of Bi <sub>2</sub> O <sub>2</sub> CO <sub>3</sub> . RSC Advances, 2016, 6, 94361-94364.	1.7	20
255	Controlling the secondary pollutant on B-doped g-C <sub>3</sub> N <sub>4</sub> during photocatalytic NO removal: a combined DRIFTS and DFT investigation. Catalysis Science and Technology, 2019, 9, 4531-4537.	2.1	20
256	High-surface energy enables efficient and stable photocatalytic toluene degradation <i>via</i> the suppression of intermediate byproducts. Catalysis Science and Technology, 2019, 9, 2952-2959.	2.1	20
257	Highly durable isotypic heterojunction generated by covalent cross-linking with organic linkers for improving visible-light-driven photocatalytic performance. Applied Catalysis B: Environmental, 2020, 260, 118182.	10.8	20
258	Mo Promotes Interfacial Interaction and Induces Oxygen Vacancies in 2D/2D of Mo-g-C <sub>3</sub> N <sub>4</sub> and Bi <sub>2</sub> O <sub>2</sub> CO <sub>3</sub> Photocatalyst for Enhanced NO Oxidation. Industrial & Engineering Chemistry Research, 2020, 59, 9509-9518.	1.8	20
259	Perovskite Nanocrystalsâ€Based Heterostructures: Synthesis Strategies, Interfacial Effects, and Photocatalytic Applications. Solar Rrl, 2021, 5, 2000419.	3.1	20
260	Photocatalytic destruction of volatile aromatic compounds by platinized titanium dioxide in relation to the relative effect of the number of methyl groups on the benzene ring. Science of the Total Environment, 2022, 822, 153605.	3.9	20
261	Unveiling the collective effects of moisture and oxygen on the photocatalytic degradation of m-Xylene using a titanium dioxide supported platinum catalyst. Chemical Engineering Journal, 2022, 439, 135747.	6.6	20
262	(NH <sub>4</sub> ) <sub>2</sub> SO <sub>4</sub> -assisted polycondensation of dicyandiamide for porous g-C <sub>3</sub> N <sub>4</sub> with enhanced photocatalytic NO removal. RSC Advances, 2016, 6, 96334-96338.	1.7	19
263	Quantifying the activation energies of ROS-induced NOx conversion: Suppressed toxic intermediates generation and clarified reaction mechanism. Chemical Engineering Journal, 2019, 375, 122026.	6.6	19
264	The structural differences of perovskite ATiO3 (AÂ=ÂCa, Sr) dictate the photocatalytic VOCs mineralization efficiency. Chemical Engineering Journal, 2021, 425, 130613.	6.6	19
265	CsPbBr <sub>3</sub> Perovskite Nanocrystal: A Robust Photocatalyst for Realizing NO Abatement. ACS ES&T Engineering, 2021, 1, 1021-1027.	3.7	18
266	Optimizing the Gas–Solid Photocatalytic Reactions for Air Purification. ACS ES&T Engineering, 2022, 2, 1103-1115.	3.7	18
267	Synthesis of flower-like, pinon-like and faceted nanoplates (BiO)2CO3 micro/nanostructures with morphology-dependent photocatalytic activity. Materials Chemistry and Physics, 2013, 142, 381-386.	2.0	17
268	Insights into peroxymonosulfate activation under visible Light: Sc2O3@C3N4 mediated photoexcited electron transfer. Chemical Engineering Journal, 2022, 435, 134836.	6.6	17
269	Design and mechanism of photocatalytic oxidation for the removal of air pollutants: a review. Environmental Chemistry Letters, 2022, 20, 2687-2708.	8.3	17
270	Light-induced secondary hydroxyl defects in Sr1-xSn(OH)6 enable sustained and efficient photocatalytic toluene mineralization. Chemical Engineering Journal, 2022, 427, 131764.	6.6	15

#	Article	IF	CITATIONS
271	B doped Bi2O2CO3 hierarchical microspheres: Enhanced photocatalytic performance and reaction mechanism for NO removal. Catalysis Today, 2021, 380, 230-236.	2.2	14
272	The mechanisms of interfacial charge transfer and photocatalysis reaction over Cs3Bi2Cl9 QD/(BiO)2CO3 heterojunction. Chemical Engineering Journal, 2022, 430, 132974.	6.6	14
273	OH/Na co-functionalized carbon nitride: directional charge transfer and enhanced photocatalytic oxidation ability. Catalysis Science and Technology, 2020, 10, 529-535.	2.1	13
274	Crystal-structure dependent reaction pathways in photocatalytic formaldehyde mineralization on BiPO4. Journal of Hazardous Materials, 2021, 420, 126633.	6.5	13
275	Self-doped Br in Bi5O7Br ultrathin nanotubes: Efficient photocatalytic NO purification and mechanism investigation. Chinese Chemical Letters, 2022, 33, 3161-3166.	4.8	13
276	A new strategy for plasma-catalytic reduction of NO to N2 on the surface of modified Bi2MoO6. Chemical Engineering Journal, 2022, 440, 135754.	6.6	13
277	Efficient NO removal and photocatalysis mechanism over Bi-metal@Bi2O2[BO2(OH)] with oxygen vacancies. Journal of Hazardous Materials, 2022, 436, 129271.	6.5	13
278	Enhanced Visible Light Photocatalytic Activity of Br-Doped Bismuth Oxide Formate Nanosheets. Molecules, 2015, 20, 19189-19202.	1.7	12
279	An ion-exchange strategy for I-doped BiOCOOH nanoplates with enhanced visible light photocatalytic NOx removal. Pure and Applied Chemistry, 2018, 90, 353-361.	0.9	12
280	Doping and facet effects synergistically mediated interfacial reaction mechanism and selectivity in photocatalytic NO abatement. Journal of Colloid and Interface Science, 2021, 604, 624-634.	5.0	12
281	Photocatalytic reaction mechanisms at the gas–solid interface for environmental and energy applications. Catalysis Science and Technology, 2021, 11, 7807-7839.	2.1	12
282	Rational Design of LDH/Zn <sub>2</sub> SnO <sub>4</sub> Heterostructures for Efficient Mineralization of Toluene Through Boosted Interfacial Charge Separation. Energy and Environmental Materials, 2023, 6, .	7.3	12
283	Lower treating temperature leading to higher air purification activity. Chemical Engineering Journal, 2017, 314, 640-649.	6.6	11
284	Promotion mechanism of –OH group intercalation for NOx purification on BiOI photocatalyst. Nanoscale, 2021, 13, 20601-20608.	2.8	10
285	Controllable synthesis of a 3D ZnS@MoO <sub>3</sub> heterojunction <i>via</i> a hydrothermal method towards efficient NO purification under visible light. CrystEngComm, 2020, 22, 257-266.	1.3	9
286	Earthâ€Abundant CaCO <sub>3</sub> â€Based Photocatalyst for Enhanced ROS Production, Toxic Byâ€Product Suppression, and Efficient NO Removal. Energy and Environmental Materials, 2022, 5, 928-934.	7.3	9
287	Crystal-Structure-Dependent Photocatalytic Redox Activity and Reaction Pathways over Ga <sub>2</sub> O <sub>3</sub> Polymorphs. ACS Applied Materials & Interfaces, 2021, 13, 50975-50987.	4.0	9
288	Enhanced Reactant Activation and Transformation for Efficient Photocatalytic Acetone Degradation on SnO <sub>2</sub> via Hf Doping. Advanced Sustainable Systems, 2021, 5, 2100115.	2.7	8

#	Article	IF	CITATIONS
289	Efficient visible light photocatalytic NO abatement over SrSn(OH)6 nanowires loaded with Ag/Ag2O cocatalyst. Environmental Research, 2021, 201, 111521.	3.7	8
290	Unraveling the Unique Role of Methyl Position on the Ring-Opening Barrier in Photocatalytic Decomposition of Xylene Isomers. ACS Catalysis, 2022, 12, 8363-8371.	5.5	8
291	Editorial: Photocatalysis for Environmental Applications. Frontiers in Chemistry, 2019, 7, 303.	1.8	7
292	Alkali/alkaline-earth metal intercalated g-C3N4 induced charge redistribution and optimized photocatalysis: status and challenges. JPhys Energy, 2021, 3, 032008.	2.3	7
293	Tuning the Morphological Structure and Photocatalytic Activity of Nitrogen-Doped (BiO) <sub>2</sub> CO <sub>3</sub> by the Hydrothermal Temperature. Journal of Nanomaterials, 2014, 2014, 1-10.	1.5	6
294	Efficient formaldehyde photo-oxidation and reaction path study on oxygen vacancy engineered TiO <sub>2</sub> . Chinese Science Bulletin, 2020, 65, 718-728.	0.4	5
295	Bismuth metal and semiconductor-based photocatalysts: structure tuning, activity enhancement, and reaction mechanism. Interface Science and Technology, 2020, 31, 349-377.	1.6	3
296	Tailoring unique neural-network-type carbon nanofibers inserted in CoP/NC polyhedra for robust hydrogen evolution reaction. Nanoscale, 2021, 13, 14705-14712.	2.8	3
297	Insights into Dynamic Surface Bromide Sites in Bi <sub>4</sub> O <sub>5</sub> Br <sub>2</sub> for Sustainable N <sub>2</sub> Photofixation. Angewandte Chemie, 0, , .	1.6	2
298	Editorial: Photocatalysts for Air Purification: Design, Synthesis, and Mechanism Investigations. Frontiers in Chemistry, 2022, 10, 870550.	1.8	1
299	Green Production of Solar Fuels Using Formaldehyde Pollutant as a Carbon Feedstock Achieving Conversion of Waste into Energy. ACS Sustainable Chemistry and Engineering, 2022, 10, 31-36.	3.2	0